

# First principles study of charge fluctuation between proximate solid state qubits

Jyh-Pin Chou and Zoltán Bodrog

*Institute for Solid State Physics and Optics, Wigner Research Centre for Physics,  
Hungarian Academy of Sciences, Budapest, POB 49, H-1525, Hungary*

Adam Gali\*

*Institute for Solid State Physics and Optics, Wigner Research Centre for Physics,  
Hungarian Academy of Sciences, Budapest, POB 49, H-1525, Hungary and*

*Department of Atomic Physics, Budapest University of Technology and Economics, Budafoki út 8, H-1111, Budapest, Hungary*

(Dated: December 14, 2024)

Point defects in solids acting as qubits are promising platform to realize quantum networks and novel nanoscale sensors. Recent advances in materials engineering make possible to create proximate qubits in solids. At too close proximity, these qubits might directly interact that deteriorate their operation. Here we demonstrate on nitrogen-vacancy (NV) qubits in diamond that first principles calculations can identify the critical distance between negatively charged and neutral NV defects at which fast charge fluctuation occurs between them, by forming an NV molecule in diamond. Our results are in quantitative agreement with recent experimental data, and pave the way for *ab initio* simulation of the interaction of solid state qubits.

Quantum bits or qubits are the building blocks of future quantum computers and nanoscale sensor devices. Special point defects with non-zero electron spin states can realize qubits in solids [1–3] that can be well engineered by different implantation or irradiation techniques [4–8]. Proximate qubits with electron-spin-electron-spin-dipole-dipole interaction may establish a quantum network in solids [9]. The negatively charged nitrogen-vacancy defect [NV(–)] (see Refs. [10, 11]) represents such a qubit in diamond [1, 12, 13]. Isolated NV(–) has a long spin coherence time of  $\approx 1.8$  ms [14] in high quality diamond samples that holds even at room temperature. This makes this qubit very attractive in biological or biomolecule sensing applications too [15] where the dense array of qubits can be very advantageous [16, 17]. The NV color center consists of a substitution nitrogen next to a carbon vacancy [see Fig. 1(a)] which creates an  $a_1$  level and a double degenerate  $e$  level in the gap that are occupied by four electrons in the negative charge state [see Fig. 1(b)]. We note that the defect can be found in its neutral charge state too [NV(0)] [18] in which the  $e$  level is only occupied by a single electron. The initialization and readout of this qubit can be done optically [see Fig. 1(c)], where the luminescence intensity of the illuminated NV center depends on the electron spin state, and subsequent optical cycles will polarize the electron spin to the  $ms = 0$  state.

Recently, NV(–) centers have been engineered with an extremely high concentration of about 45 ppm by means of subsequent electron irradiation and annealing of nitrogen contaminated diamond [7, 8], that resulted in a strong long-range magnetic dipolar interaction of  $(2\pi)420$  kHz between them. That might be the base of quantum network study. However, it has been found [7] that the electron spin coherence time significantly reduces to about  $67 \mu\text{s}$  in this sample. A charge fluctua-

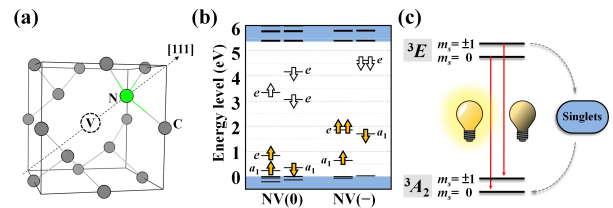


FIG. 1. Nitrogen-vacancy (NV) defect in diamond. (a) Optimized geometry in the core of NV center. (b) Single particle defect levels in the fundamental band gap in the ground state of NV(–). (c) Many-body levels at room temperature and decay from the optically active  $^3E$  excited state to the  $^3A_2$  groundstate. Radiative (non-radiative) transitions are depicted by straight (dashed-curved) arrows. Bright (dark) lamp illustrates the most (less) intense fluorescence of NV center that is the base of optical spinpolarization and readout of the  $ms$  electron spin state.

tion model was developed between neighbor NV(–) and NV(0) defects with about an average distance of 5 nm that lead to the decoherence of NV(–) spin state. The charge fluctuation characteristic time was estimated to  $\tau = 10$  ns in this diamond sample, that corresponded well to the estimated spin depolarization frequency of  $(2\pi)3.3$  MHz. These estimations were based on point dipole model of the spin that might be oversimplification as previous density functional theory (DFT) calculations showed [19] that the electron density distribution of the NV center is strongly anisotropic. First principles investigation of direct interaction between proximate NV defects is of high importance that can lead to understanding this particular qubit and provide a recipe to study other color center qubits in solids.

In this Letter, we study the interaction between neighbor negatively charged and neutral NV defects in diamond as a function of their distance by means of *ab initio*

calculations with realistically large models of thousands of atoms. Our calculations imply a direct tunneling of the charge of NV(-) toward NV(0) where the probability of the tunneling or hopping is directional dependent in diamond. The calculated average hopping time of  $\tau \approx 10$  ns at  $\approx 4.4$  nm distance of various NV pair configurations in the diamond lattice is in good agreement with the previously deduced experimental data that was based on the charge fluctuation model. We find that a neighbor single NV pair may be considered as [NV-NV](-) molecule where a single electron binds the two NV defects. By extrapolating from our *ab initio* data we estimate that an average distance of  $\approx 6.4$  nm between the NV(0)-NV(-) pairs results in stable individual NV(-) at least for  $100\times$  repetitive optical cycles.

Our first principles approach is based on plane-wave supercell Kohn-Sham DFT[20, 21] calculations on NV defect as implemented in VASP code [22] with the projector augmented wave (PAW) method [23]. To model the NV defect, we applied extremely large supercell with thousands of atoms that will be discussed below. The large supercells suffice to use  $\Gamma$ -point sampling of the Brillouin-zone for converged electron density and real Kohn-Sham wavefunctions. The plane wave cutoff was set to 370 eV [24]. We applied Perdew-Burke-Ernzerhof (PBE) DFT exchange-correlation functional [25] that provides fairly accurate wavefunctions in the groundstate of NV defects [26, 27]. We projected the values of the Kohn-Sham defect wavefunctions to the three-dimensional (3D) equidistant grid within the applied supercell with  $\approx 0.31$  Å distances between the grid points. The geometry of the NV defects were optimized within PBE DFT calculations where the quantum mechanical forces acting on atoms in the optimized geometries were below 0.01 eV/Å.

We first studied a neighbor NV(-)-NV(0) pair in a  $8 \times 8 \times 8$  Bravais cubic diamond supercell with lattice constant of 2.84 nm and 4096 atoms, where the NV defects were situated in the corner and the center of this supercell with a corresponding distance of 2.46 nm. We found by DFT calculations that the lowest energy electronic structure shows a shared electron between the two NV defects, so one electron from the  $e$  orbitals of NV(-) that was originally localized on NV(-), will be localized on both NV defects creating an [NV-NV](-) unit. This interaction of the two neighbor NV defects may be considered as bonding of two NV “atoms” forming an NV-NV “molecule”. This effect can be also considered as the electron jumps back and forth between the original NV(-) and NV(0). The electron carries a charge and spin, thus this jumping electron represents the charge fluctuation of NV(-) and also affect the electron spin coherence time of NV(-). This is basically consistent with the charge fluctuation model developed previously [7]. On the other hand, one has to realize that the electron in the  $e$  orbital has a special shape and extension around the NV defect in both charge states (see Fig. 2). As a

consequence, the hopping frequency between the two NV defects should depend on the relative orientations of the two NV defects and the extension of the corresponding wavefunctions at a given distance.

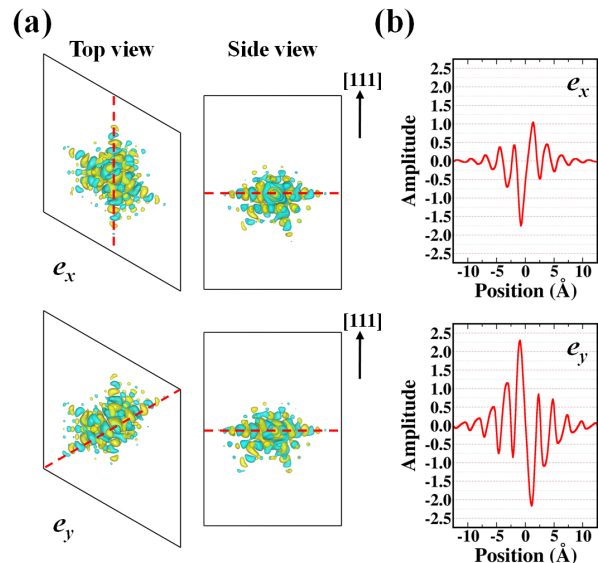


FIG. 2. (a) Top and side view of the  $e_x$  and  $e_y$  defect wavefunctions of the negatively charged NV defect in hexagonal supercell of diamond (see text). For the sake of clarity, the atoms are not shown in diamond. The real space wavefunctions are visualized: the green and yellow lobes represent the isosurface of the wavefunction at values of  $+1.89 \times 10^{-6} 1/\text{\AA}^3$  and  $-1.89 \times 10^{-6} 1/\text{\AA}^3$  values, respectively. (b) The wavefunction amplitude profile along the dashed line in (a) panel. The origo is set to the middle of the dashed line.

We conclude that the hopping frequency should be calculated *ab initio*. To this end, we set up a simple model. We assume two interacting defects, at site  $A$  and site  $B$ . In the isolated case, i.e., the distance between  $A$  and  $B$  is large, and the corresponding wavefunctions are localized at site  $A$  ( $\psi_A$ ) and site  $B$  ( $\psi_B$ ). By approaching the defects, the electron may tunnel from site  $A$  to site  $B$ , and the defects form a special molecule-like defect complex. This description is similar to the tight binding theory of covalent bonds. The hopping rate between the two sites ( $\Omega_{AB}$ ) may be calculated as

$$\Omega_{AB} \approx \frac{1}{\hbar} \langle \psi_A | \hat{H}_{AB} | \psi_B \rangle \approx \frac{E_0}{\hbar} \langle \psi_A | \psi_B \rangle \quad (1)$$

where  $\hat{H}$  is an effective single particle Hamiltonian acting on the electron that binds the two sites,  $r$  is the distance between two defects, and  $\hbar$  is the Planck-constant. The integral can be approximated by the overlap integral of the real wavefunctions at  $A$  and  $B$  sites ( $\langle \psi_A | \psi_B \rangle$ ) multiplied by  $E_0$  where the latter is related to an average energy of the two sites [28]. This leads to an exponential decay of the hopping rate as a distance between the two

sites. We calculated these two quantities *ab initio* with applying different strategies and supercells.

First, we discuss the calculation of the overlap integral. Because of the shape of electron density distribution of the  $e$  orbital of the NV defect (see Fig. 2), it is convenient to apply hexagonal supercell that is commensurate with the  $C_{3v}$  symmetry of the defect, and the  $z$ -axis of the supercell lies parallel to the NV-axis, i.e.,  $\langle 111 \rangle$  direction. By this construction, the interactions between defect wavefunctions can be individually studied on the (111) basal plane and perpendicular to it, in a straightforward manner. We plotted the DFT wavefunctions in  $10 \times 10 \times 5$  hexagonal supercell of diamond in Fig. 2, with  $25.1 \text{ \AA} \times 25.1 \text{ \AA} \times 30.7 \text{ \AA}$  lattice constants and 3000 atoms. We checked that the calculated Kohn-Sham levels and wavefunctions of NV(-) and NV(0) in the gap agree with those obtained in the  $8 \times 8 \times 8$  cubic supercell (see in Ref. 29). The line profiles in Fig. 2(b) show that the wavefunction propagation almost vanishes at the hexagonal cell boundary. We found that the decay of the wavefunctions is relatively fast and the electron probability  $|\psi|^2$  is about 0.1% at a distance of 1 nm away from NV center. Thus, the direct interaction between the NV periodic images is very small in this supercell, and has a very tiny influence on the Kohn-Sham defect levels, showing basically zero dispersion in the Brillouin-zone (see more details in Ref. 29). We note that the same conclusion was achieved for the  $e_x$  and  $e_y$  defect states of NV(0). This means that our chosen hexagonal supercell accommodates NV defect as isolated defect, as the interaction with its periodic images is virtually zero. Therefore, the calculated DFT wavefunctions in this supercell and the corresponding 3D grid can be taken as a cluster of an isolated defect. We calculated the DFT wavefunctions for NV(-) and NV(0) situated in the middle of this supercell, and then we stored the corresponding  $e$  wavefunctions on the 3D grid in each calculation. In this construction, we could reach 5.2 nm maximum distance between the two NV defects in the (111) plane. By taking the clusters of NV(-) and NV(0), the corresponding overlap integral can be calculated at various distances and all the possible NV-NV orientations within the range of maximum distance.

Second, estimation of  $E_0$  requires further consideration. This can be done by noting that a similar  $H_{AB}$  hopping integral appears in the tight binding approximation of bonds in solids. This can be employed to determine an approximate  $E_0$ . We note that the electron is completely shared in  $[\text{NV-NV}](-)$  unit according to our *ab initio* calculation, thus this can be considered as NV(-1/2) defect on the two sites, where (-1/2) means half charge (half electron). By calculating the array of NV(-1/2) units in diamond with a given lattice constant between NV(-1/2) units, once  $H_{AB}$  integral value is inferred from DFT calculation, one can calculate the overlap integral between the two sites at that distance

between NV(-1/2) defects (as explained above), and finally  $E_0$  can be calculated as a division of  $H_{AB}$  integral value and this overlap integral value. In order to derive the  $H_{AB}$  integral value in this system, we applied tight binding theory to it with using  $C_{3v}$  symmetry. Indeed, exactly the same type of hopping integral  $t$  appears as shown in Eq. 1 (see Ref. 29).

We demonstrate this procedure on Fig. 3. We choose the cubic array of NV defect with a half extra charge in a  $4 \times 4 \times 4$  cubic supercell where the dispersion relation is studied along  $[100]$ ,  $[010]$ ,  $[001]$ ,  $[110]$ ,  $[101]$ ,  $[011]$ ,  $[111]$ ,  $[\bar{1}11]$ ,  $[1\bar{1}1]$ , and  $[11\bar{1}]$  directions in the Brillouin zone (details are shown in Ref. 29). According to our derivation based on tight binding theory, the maximum dispersion of the half-occupied  $e_y$  orbital along  $[100]$  direction of the Brillouin zone depends on  $t$  that can be directly calculated by DFT electronic structure calculations. The  $4 \times 4 \times 4$  cubic supercell yields small dispersion for the important half-filled  $e_y$  level (see Fig. 3) which indicates that the direct interaction between the periodic images is very small but still sufficiently large to be above the numerical uncertainty of  $\approx 1$  meV. The tight binding retrofit to the  $e_y$  level is almost perfect with a standard deviation of about 1%. The overlap between the wavefunctions at this orientation and distance of NV defects can be calculated by taking the hexagonal clusters as explained above. Finally, we obtain  $E_0 = 0.058$  eV (see Ref. 29).

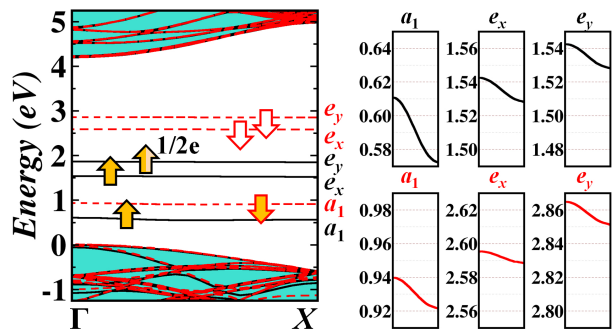


FIG. 3. The band structure of NV defect in a  $4 \times 4 \times 4$  cubic cell along  $\Gamma(0,0,0)$  point to  $X(1/2,0,0)$  point with half extra charge. The valence band maximum is aligned to zero level. The calculations were carried by PBE DFT functional that provides inaccurate band gap but the Kohn-Sham wavefunctions should be accurate. Because of the half charge the symmetry is tilted a bit to  $C_{1h}$  symmetry, thus  $e_x$  and  $e_y$  levels slightly split but it is very close to the  $C_{3v}$  symmetry. The spinpolarized PBE DFT calculations results in separate spin-up (black straight curve) and spin-down (red dotted curve) bands and levels. The valence and conduction band regions are colored by green. The orange and white arrows represent the occupied and unoccupied defect states, respectively. The six panels show the dispersion of each in-gap defect levels in the region  $\Gamma$ - $X$ . The hopping integral was inferred from the dispersion of the half electron ( $1/2e$ ) filled  $e_y$  level.

By having the value of  $E_0$  in our hand, we calculated the corresponding overlap integral at various distances (up to 5.2 nm) and all the possible NV–NV orientations when accessible in the combination of the applied hexagonal clusters. It is apparent from Fig. 2(a) that the overlap of wavefunctions should be larger on the NV–NV orientation of (111) plane than that in other NV–NV orientations. Consequently, the individual hopping rates will be also larger for the corresponding NV–NV orientations. The schematic illustration of NV(–)–NV(0) configurations along 26 directions around the target NV are shown in Fig. 4(a), and all the corresponding hopping rates are calculated and summarized in Fig. 4(b). By fitting the hopping rate to an exponential regression in the range from 1.5 nm to 5.2 nm, we found that the hopping rate is around  $(2\pi)13$  MHz on average at 4.4 nm distance between NV defects that corresponds to  $\approx 10$  ns diffusion time. This is in the order of magnitude of the optical lifetime for the negatively charged NV defect in diamond[30], and can explain the charge fluctuation in diamond with high NV concentration. Our calculations are in very good agreement with previous studies on such diamond samples [7]. The derived hopping rate goes as  $(2\pi)2.30 \times 10^{14} \exp(-0.38r)$  Hz by fitting to the results [blue line in Fig. 4(b)], where distance  $r$  is given in Ångström unit. By extrapolating the hopping rate with this formula, we find that minimum  $100\times$  repetitive optical cycle can be carried out when the neighbor NV(0) defect resides at  $\approx 6.4$  nm distance from the NV(–). This average distance corresponds to  $\approx(2\pi)200$  kHz dipole-dipole interaction among NV qubits for quantum network applications.

In conclusion, we carried out *ab initio* calculations to study charge fluctuation between solid state qubits, in particular, the NV defects in diamond. We found that the electron can tunnel between proximate NV(–) and NV(0) defects. We provided detailed quantitative analysis on the probability of tunneling or hopping as a function of orientation and distance between the NV defects. Our findings are in quantitative agreement with data from previous studies. We identified the critical distance between NV defects for optical repetitive readout of single NV qubit. Our conclusions are important in future quantum network and sensing studies of this solid state qubit. Our *ab initio* methodology for studying charge and spin fluctuation of proximate qubits can be applied for other solid state qubit systems.

We acknowledge the funding support from the EU Commission FP7 grant No. 611143 (DIADEMS) and from the MTA Lendület programme from Hungarian Academy of Sciences.

\* gali.adam@wigner.mta.hu

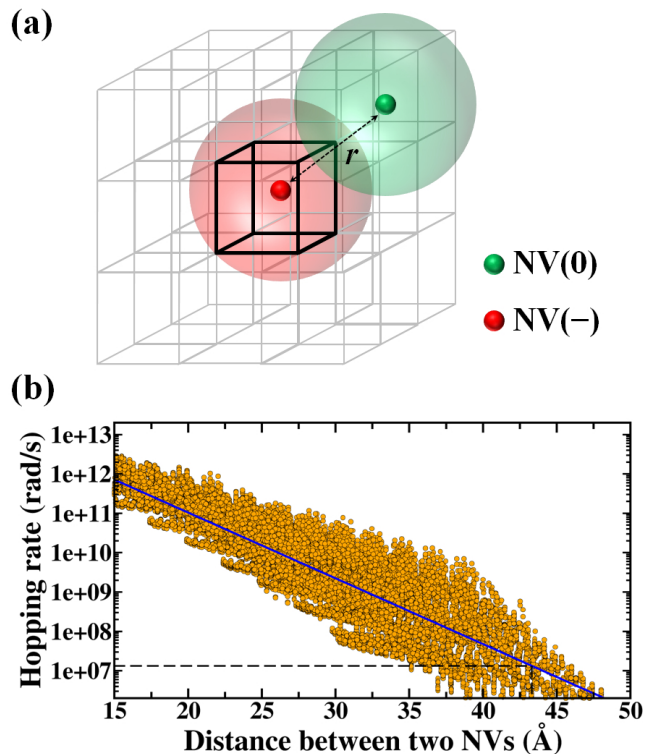


FIG. 4. (a) Schematic illustration of two NV centers with the separation of  $r$ . The wavefunction of NV is converted into a 3-dimensional equidistant grid. The maximum of separation  $r$  in this hexagonal cell is 5.2 nm in the (111) plane. (b) The calculated hopping rate of electrons of all possible configurations at a given distance  $r$ . The average hopping rate values are shown as a blue line. We note that all the possible configurations could be taken into account for  $r \leq 4.5$  nm. For larger  $r$  we have only subset of configurations because of the constraint of the size and shape of the hexagonal cluster. The value of the hopping rate can be extrapolated at larger  $r$  by assuming an overall exponential decay. The dashed horizontal line shows a critical rate at  $(2\pi)13.2$  MHz which is the deduced rate of the radiative decay (see Ref. 31).

- [1] L. Childress, M. V. G. Dutt, J. M. Taylor, A. S. Zibrov, F. Jelezko, J. Wrachtrup, P. R. Hemmer, and M. D. Lukin, *Science* **314**, 281 (2016).
- [2] W. F. Koehl, B. B. Buckley, F. J. Heremans, G. Calusine, and D. D. Awschalom, *Nature* **479**, 84 (2011).
- [3] J. J. Pla, K. Y. Tan, J. P. Dehollain, W. H. Lim, J. J. L. Morton, D. N. Jamieson, A. S. Dzurak, and A. Morello, *Nature* **489**, 541 (2012).
- [4] D. M. Toyli, C. D. Weis, G. D. Fuchs, T. Schenkel, and D. D. Awschalom, *Nano Lett.* **10**, 3168 (2010).
- [5] A. L. Falk, B. B. Buckley, G. Calusine, W. F. Koehl, V. V. Dobrovitski, A. Politi, C. A. Zorman, P. X.-L. Feng, and D. D. Awschalom, *Nat. Commun.* **4** (2013), 10.1038/ncomms2854.
- [6] J. T. Muhonen, J. P. Dehollain, A. Laucht, F. E. Hudson, R. Kalra, T. Sekiguchi, K. M. Itoh, D. N. Jamieson, J. C. McCallum, A. S. Dzurak, and A. Morello, *Nat. Nanotech.* **9**, 986 (2014).
- [7] J. Choi, S. Choi, G. Kucsko, P. C. Maurer, B. J. Shields,



- H. Sumiya, S. Onoda, J. Isoya, E. Demler, F. Jelezko, N. Y. Yao, and M. D. Lukin, *Phys. Rev. Lett.* **118**, 093601 (2017).
- [8] S. Choi, J. Choi, R. Landig, G. Kucsko, H. Zhou, J. Isoya, F. Jelezko, S. Onoda, H. Sumiya, V. Khemani, C. von Keyserlingk, N. Y. Yao, E. Demler, and M. D. Lukin, *Nature* **543**, 221 (2017).
- [9] W. Pfaff, B. J. Hensen, H. Bernien, S. B. v. Dam, M. S. Blok, T. H. Taminiau, M. J. Tiggelman, R. N. Schouten, M. Markham, D. J. Twitchen, and R. Hanson, *Science* **345**, 532 (2014).
- [10] L. Du Preez, *Electron paramagnetic resonance and optical investigations of defect centres in diamond*, Ph.D. thesis, University of the Witwatersrand, Johannesburg (1965).
- [11] G. Davies and M. F. Hamer, *Proc. R. Soc. London Ser. A* **348**, 285 (1976).
- [12] A. Gruber, A. Dräbenstedt, C. Tietz, L. Fleury, J. Wrachtrup, and C. von Borczyskowski, *Science* **276**, 2012 (1997).
- [13] F. Jelezko, T. Gaebel, I. Popa, A. Gruber, and J. Wrachtrup, *Phys. Rev. Lett.* **92**, 076401 (2004).
- [14] G. Balasubramanian, P. Neumann, D. Twitchen, M. Markham, R. Kolesov, N. Mizuochi, J. Isoya, J. Achard, J. Beck, J. Tissler, V. Jacques, P. R. Hemmer, F. Jelezko, and J. Wrachtrup, *Nat. Mater.* **8**, 383 (2009).
- [15] S. J. DeVience, L. M. Pham, I. Lovchinsky, A. O. Sushkov, N. Bar-Gill, C. Belthangady, F. Casola, M. Corbett, H. Zhang, M. Lukin, H. Park, A. Yacoby, and R. L. Walsworth, *Nat. Nanotech.* **10**, 129 (2015).
- [16] J. M. Taylor, P. Cappellaro, L. Childress, L. Jiang, D. Budker, P. R. Hemmer, A. Yacoby, R. Walsworth, and M. D. Lukin, *Nat. Phys.* **4**, 810 (2008).
- [17] V. M. Acosta, E. Bauch, M. P. Ledbetter, C. Santori, K.-M. C. Fu, P. E. Barclay, R. G. Beausoleil, H. Linget, J. F. Roch, F. Treussart, S. Chemerisov, W. Gawlik, and D. Budker, *Phys. Rev. B* **80**, 115202 (2009).
- [18] K. Beha, A. Batalov, N. B. Manson, R. Bratschitsch, and A. Leitenstorfer, *Phys. Rev. Lett.* **109**, 097404 (2012).
- [19] A. Gali, M. Fyta, and E. Kaxiras, *Phys. Rev. B* **77**, 155206 (2008).
- [20] P. Hohenberg and W. Kohn, *Phys. Rev.* **136**, B864 (1964).
- [21] W. Kohn and L. J. Sham, *Phys. Rev.* **140**, A1133 (19654).
- [22] G. Kresse and J. Furthmüller, *Phys. Rev. B* **54**, 11169 (1996).
- [23] P. E. Blöchl, *Phys. Rev. B* **50**, 17953 (1994).
- [24] P. Deák, B. Aradi, M. Kaviani, T. Frauenheim, and A. Gali, *Phys. Rev. B* **89**, 075203 (2014).
- [25] J. P. Perdew, K. Burke, and M. Ernzerhof, *Phys. Rev. Lett.* **77**, 3865 (1996).
- [26] A. Gali, *Phys. Rev. B* **79**, 235210 (2009).
- [27] K. Szász, T. Hornos, M. Marsman, and A. Gali, *Phys. Rev. B* **88**, 075202 (2013).
- [28] R. S. Mulliken, *J. Chim. Phys. Physicochim. Biol.* **46**, 497 (1949).
- [29] See Supplementary Material at <http://...> for details about the technicalities of the supercell method, and the tight binding calculations.
- [30] F. Jelezko and J. Wrachtrup, *physica status solidi (a)* **203**, 3207 (2006).
- [31] M. L. Goldman, A. Sipahigil, M. W. Doherty, N. Y. Yao, S. D. Bennett, M. Markham, D. J. Twitchen, N. B. Manson, A. Kubanek, and M. D. Lukin, *Phys. Rev. Lett.* **114**, 145502 (2015).